RSC Advances

PAPER

View Article Online
View Journal | View Issue

Cite this: *RSC Adv.*, 2017, **7**, 51142

An Fe_3O_4@P4VP@$FeCl_3$ core–shell heterogeneous catalyst for aerobic oxidation of alcohols and benzylic oxidation reaction†

Ruilian Li,[a] Jian Zhao,[b] Fengxia Yang,[b] Yingchao Zhang,[b] Daniele Ramella,[c] Yu Peng *[a] and Yi Luan *[b]

Received 15th August 2017
Accepted 29th October 2017

DOI: 10.1039/c7ra09005f

rsc.li/rsc-advances

A novel magnetic Fe_3O_4@P4VP(poly(4-vinylpyridine))@$FeCl_3$ core–shell structure was successfully synthesized. Its Fe_3O_4@P4VP core was initially prepared *via* polymerization of 4-vinyl pyridine on the surface of Fe_3O_4 microspheres. The successful introduction of the $FeCl_3$ moiety as a catalytic active site was achieved through coordination interaction between P4VP and $FeCl_3$. The obtained Fe_3O_4@P4VP@$FeCl_3$ catalyst was applied in the selective oxidation of alcohols using molecular oxygen as the oxidant. It was shown that a variety of alcohol substrates is tolerated under optimized reaction conditions. Additionally, benzylic oxidation of hydrocarbon compounds was also evaluated using Fe_3O_4@P4VP@$FeCl_3$ as the catalyst and *t*BuOOH as the oxidant, achieving high yields and very good selectivities. The heterogeneity of the Fe_3O_4@P4VP@$FeCl_3$ core–shell catalyst was tested and the initial activity was maintained after five reuses.

1. Introduction

The catalytic selective oxidation of alcohols to the corresponding carbonyl compounds is one of the most industrially significant reactions in fine and industrial organic chemistry.[1] The use of transition metal-based homogeneous[2] and heterogeneous[3] catalysts is a good strategy as the use of stoichiometric oxidants such as chromate or permanganate is replaced by atom-economical clean oxidants. However, heterogeneous processes are preferable for oxidation, as they display several advantages during the purification and recovery steps of products and catalysts.[4] Oxidizing alcohols heterogeneously using molecular oxygen is an ideal reaction process, since it produces H_2O as the sole by-product.[5] Recently, aerobic oxidations received much attention because of their use of inexpensive oxidants and controllable selectivities. Studies about homogenous catalysts for aerobic oxidation reactions are abundant in the literature.[6] Several successful noble metal catalytic systems, such as gold,[7] palladium,[8] platinum,[9] rhodium,[10] ruthenium,[11] *etc.* were reported for having achieved efficient oxidation of alcohols.

Over the years, the utilization of relatively inexpensive transitional metals like copper or iron have been considered an approach towards the replacement of such expensive precious metal catalysts. Although copper derived catalysts have been studied thoroughly over the years as an alternative to platinum-based ones in the oxidation of alcohols,[12] iron derived ones remain relatively underexplored. Iron is less expensive and more naturally abundant than copper and other transitional metals. Since the first iron-promoted oxidation of alcohols was reported in 2002,[13] this field witnessed an increase in iron use for the promotion of oxidation reactions. Wang and coworkers reported a $FeCl_3$-TEMPO-$NaNO_2$ system,[14] while Ma and colleagues have published an $Fe(NO_3)_3$-TEMPO-NaCl system[15] for oxidation reactions. However, homogeneous iron catalytic systems make the recovery of the catalyst extremely difficult, which might pose limitations to industrial scale applications. Thus, in recent years, numerous heterogeneous supports, such as molecular sieves,[16] aluminosilicates,[17] graphene-oxide[18] polymer[19] and inorganic microspheres, have been developed and applied to the alcohol oxidation reaction.[20]

Although heterogeneous iron catalysts were achieved in a stable and reusable manner, they commonly showed lower efficiency and metal leaching compared to their homogeneous counterparts. Among these heterogeneous catalysts, core–shell structures have been considered highly practical as they take advantage of their unique physicochemical and multifunctional properties.[21] Magnetic core-shell structures are of particular interest as an effective separation method since they could easily and quickly respond to an external magnetic field.[22] Many magnetic core–shell composites have been developed

[a]*Hunan Agricultural University, Hunan, 410128, P. R. China. E-mail: pengy7505@hunau.net; Tel: +86-731-84617022*

[b]*School of Materials Science and Engineering, University of Science and Technology Beijing, 30 Xueyuan Road, Haidian District, Beijing 100083, P. R. China. E-mail: yiluan@ustb.edu.cn*

[c]*Temple University-Beury Hall, 1901, N. 13th Street, Philadelphia, PA 19122, USA*

† Electronic supplementary information (ESI) available. See DOI: 10.1039/c7ra09005f

utilizing different coatings, such as silica, carbon, polymeric and porous materials on a Fe_3O_4 core.[23] Several hybrid magnetic core–shell nanocatalysts have been utilized in reductions, oxidations, epoxidations, coupling reactions and photo-catalytic reactions.[24] To the best of our knowledge, the combination of magnetic functionality and iron catalytic sites have not been reported in the literature yet. In this work, a core–shell Fe_3O_4@P4VP@$FeCl_3$ catalyst was synthesized and it was characterized by transmission electron microscopy (TEM), powder X-ray diffraction (PXRD), FTIR spectroscopy, thermogravimetric analysis (TGA) and vibrating sample magnetometry (VSM). Numerous pyridine functional groups provided multi-dentate coordination to the iron(III) ion, which helps stabilizing the metal center. The aerobic oxidation of alcohols and benzylic carbons were both investigated using our synthesized Fe_3O_4@P4VP@$FeCl_3$ catalyst. High chemical stability and low metal leaching were observed for the oxidation catalysis using our core–shell catalyst.

2. Experimental section

2.1 General information

All reaction substrates and solvents were purchased from Sigma–Aldrich, Alfa Aesar or Aladdin. Ferric chloride hexahydrate ($FeCl_3 \cdot 6H_2O$), polyvinyl pyrrolidone (PVP; $M_r = 58\,000$), divinylbenzene (DVB, 80%), potassium persulfate (KPS, 99%) were purchased from Alfa Aesar and were used as received. Poly(acrylic acid) (PAA; $M_r = 1800$) and 2,2′-azobis (2-methylpropionamidine) dihydrochloride (97%) were purchased from Sigma–Aldrich. Anhydrous sodium acetate (99%) was supplied by Aladdin. 4-Vinylpyridine monomer (96%, 4VP; Aldrich) was stabilized with 100 ppm hydroquinone and used after distillation.

2.2 Characterization

The morphology and size of the as-obtained samples were characterized on a ZEISS SUPRA55 scanning electron microscopy (FESEM). High-resolution transmission electron microscopy (HRTEM) studies were carried out on a JEOL JEM 2010 transmission electron microscope with an accelerating voltage of 200 kV. The phase structure was determined by powder X-ray diffraction (p-XRD) experiments on a DSADVANCE diffractometer with Cu Kα radiation scanning from 10° to 80°. Fourier-transformed infrared spectra (FTIR) were recorded using a NICOLET 6700 infrared spectrophotometer using KBr pellet samples. The magnetization curves of samples were measured by a MPMS-XL superconducting quantum interference device (SQUID) at room temperature. The thermogravimetric analysis (TGA) was carried out on a NETZSCH STAf409 at a heating rate of 10 °C min^{-1} under nitrogen. X-ray photoelectron spectroscopy data were obtained with a PHI Quantera SXM. Gas chromatography-mass spectrum was recorded using Agilent 7890A/5975C. Products were determined by GC-MS using internal standard technique, and nitrobenzene was used as an internal standard.

2.3 Synthesis of the Fe_3O_4@P4VP materials

The PAA-modified Fe_3O_4 nanoparticles were prepared through an improved one-step solvothermal method reported in the literature.[25] In a typical procedure, $FeCl_3 \cdot 6H_2O$ (1.08 g), PAA (0.108 g), and sodium acetate (9 g) were all dissolved in ethylene glycol (40 mL) to form a homogeneous solution. Then, the solution was transferred to a 50 mL Teflon-lined stainless-steel autoclave and maintained at 200 °C for 12 h. After being cooled to room temperature, the obtained black products were washed with deionized water and ethanol several times, and then dried in a vacuum for 12 h. The core–shell Fe_3O_4@P4VP microspheres were prepared as follows: PAA-modified Fe_3O_4 (0.1 g) was dispersed with PVP (0.15 g) in 100 mL deionized water under ultrasonication. After being transferred into a 250 mL four-necked flask, an emulsion contained PVP (0.05 g), 4-VP (0.125 g), DVB (0.125 g), and deionized water (20 mL) were added. All of the solution was bubbled with nitrogen for 12 h under stirring. When the temperature was raised to 70 °C, a KPS solution (0.25 mL, 0.04 g mL^{-1}) was added into the reaction system. After 4 h of polymerization, the obtained products were washed with ethanol several times and dried under vacuum for 12 h.

2.4 Synthesis of the Fe_3O_4@P4VP@$FeCl_3$

5.0 g Fe_3O_4@P4VP nanoparticles were dispersed in 100 mL of $FeCl_3 \cdot 6H_2O$ ethanol solution (0.2 M). The solution was stirred for 12 h at 70 °C in an oil bath. The sample was recovered using a permanent magnet and washed with ethanol, and dried under vacuum at 80 °C. The amount of iron was analyzed by inductively coupled plasma-atomic emission spectrometry (ICP-AES); the contents of iron in Fe_3O_4@P4VP@$FeCl_3$ was determined to be 4.36 wt%.

2.5 General procedure for the aerobic oxidation of alcohol

In general, the catalytic reaction was carried out under the following conditions: 2 mol% Fe_3O_4@P4VP@$FeCl_3$ core–shell catalyst (mole percent was based on iron), 0.1 mmol $NaNO_2$, 0.2 mmol of 2,2,6,6-tetramethylpiperidine-*N*-oxyl (TEMPO) and 1.0 mmol alcohol were mixed in 2.5 mL of CH_3CN. The air in the catalytic reaction system was evacuated and oxygen gas was supplied through an O_2 balloon. After each catalytic cycle, the solution was magnetically separated and the filtered liquid solution was analysed *via* gas chromatography-mass spectrometry using nitrobenzene as the internal standard.

2.6 General procedure for the oxidation of hydrocarbon compounds

In general, a mixture of 2 mol% Fe_3O_4@P4VP@$FeCl_3$ core–shell catalyst (mole percent was based on iron), 1.0 mmol of diphenylmethane, *tert*-butyl hydroperoxide (TBHP, 5.0–6.0 M in decane, 545.0 μL, 3.0 mmol) and 1.0 mL acetonitrile was mixed in a 25 mL single-necked flask fitted with a reflux condenser. The mixture was heated at 80 °C for 24 h under air atmosphere in an oil bath. After each catalytic cycle, the solution was magnetically separated and the filtered liquid solution was analysed *via* gas chromatography-mass spectrometry using nitrobenzene as the internal standard.

2.7 Leaching test

The Fe_3O_4@P4VP@$FeCl_3$ core–shell catalyst was magnetically separated after 4 h reaction time, the conversion of benzyl alcohol and selectivity of benzaldehyde was tested by GC/MS using nitrobenzene as the internal standard. The mixture was further stirred for an additional 8 hours. After the reaction, products were again analysed by GC/MS using nitrobenzene as the internal standard.

3. Results and discussion

The Fe_3O_4 microspheres modified with PAA were synthesized by a solvothermal method reported in literature.[25] These microspheres were composed of tiny Fe_3O_4 nanocrystals within 10 nm (Fig. 2a). The P4VP shell was successfully grafted on Fe_3O_4 to form core–shell composite microspheres held together by hydrogen bonds between carboxylic groups of PAA chains and pyridine. The diameters of the magnetic core and polymer shell were about 200 and 38 nm, respectively (Fig. 2b). Furthermore, the SEM images show that Fe_3O_4 and Fe_3O_4@P4VP microspheres are monodispersed with a narrow size distribution of about 200 nm and 280 nm, respectively (Fig. 2c and d).

Fe_3O_4@P4VP@$FeCl_3$ core–shell catalysts were successfully prepared taking advantage of the multi-dentate coordination between $FeCl_3$ and poly(4-vinylpyridine) (Fig. 1). Several nitrogen sites on poly(4-vinylpyridine) ensures the stability of Fe^{3+} ions on the surface of the core–shell structure. The EDX elemental maps further provides the firm evidence of the synthesis of Fe_3O_4@P4VP@$FeCl_3$ (Fig. 3). Fe_3O_4 nanoparticles were encapsulated into polymer shells, and the iron(III) was well grafted on the surface of Fe_3O_4@P4VP. The iron elemental maps of the Fe_3O_4@P4VP@$FeCl_3$ also demonstrated an excellent distribution of iron content on the surface. The existence of iron content in the Fe_3O_4 core structure was also observed, as shown in Fig. 3.

Wide-angle p-XRD spectra of Fe_3O_4 nanoparticles, Fe_3O_4@P4VP core/shell nanospheres, and Fe_3O_4@P4VP@$FeCl_3$ core–shell structure were collected and shown in Fig. 4. The diffraction peaks of Fe_3O_4 (Fig. 4a) agree with standard JCPDS 75-1609.39 indicating a face-centered cubic lattice. After coating with P4VP, the peaks of the core–shell Fe_3O_4@P4VP microspheres are highly similar as those for Fe_3O_4 due to the low-

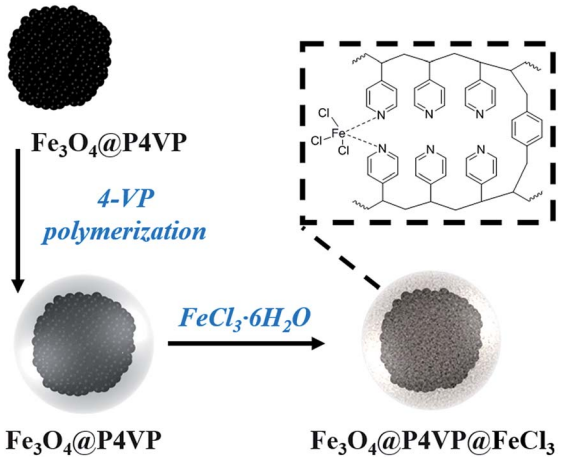

Fig. 1 Schematic illustration of the synthesis of Fe_3O_4@P4VP@$FeCl_3$.

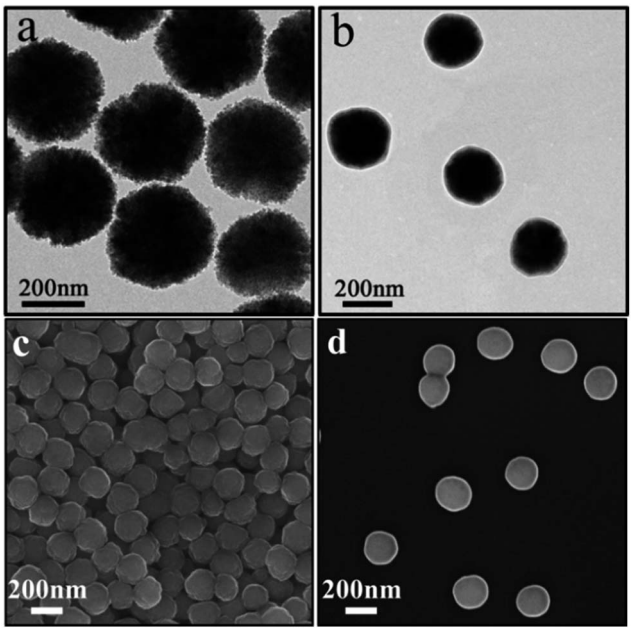

Fig. 2 TEM images of (a) Fe_3O_4, (b) Fe_3O_4@P4VP; SEM images of (c) Fe_3O_4, (d) Fe_3O_4@P4VP.

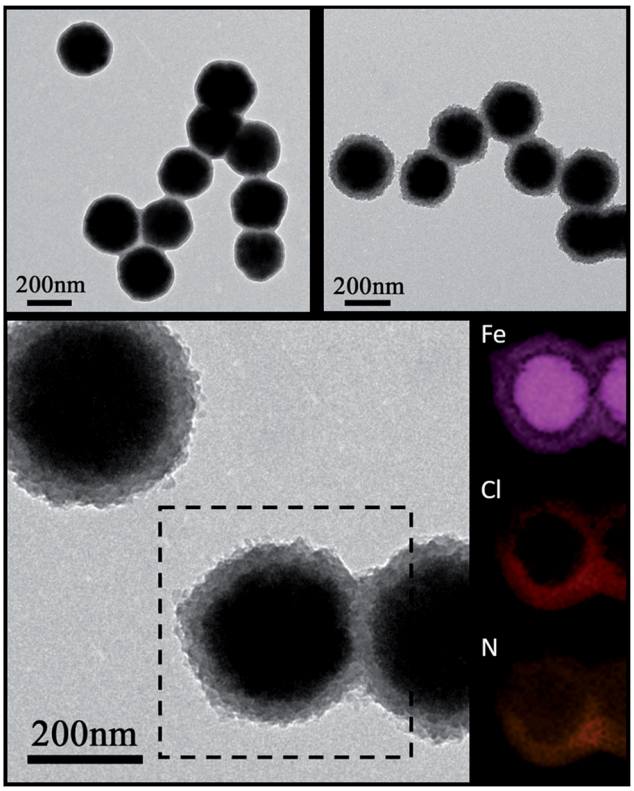

Fig. 3 HRTEM images of the Fe_3O_4@P4VP@$FeCl_3$ and EDX elemental maps of Fe, Cl and N, respectively.

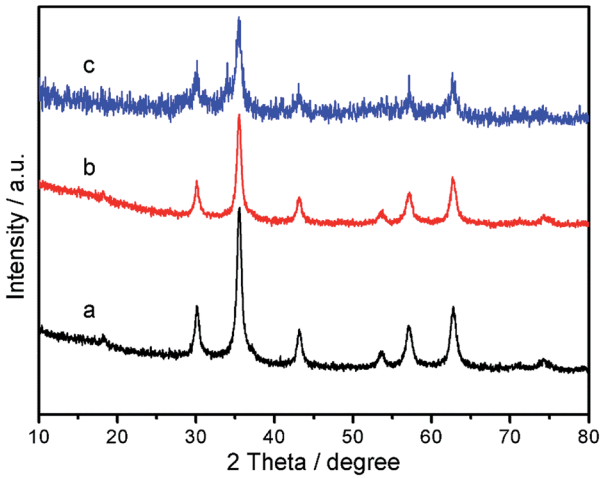

Fig. 4 PXRD patterns of (a) Fe_3O_4, (b) Fe_3O_4@P4VP and (c) Fe_3O_4@P4VP@$FeCl_3$.

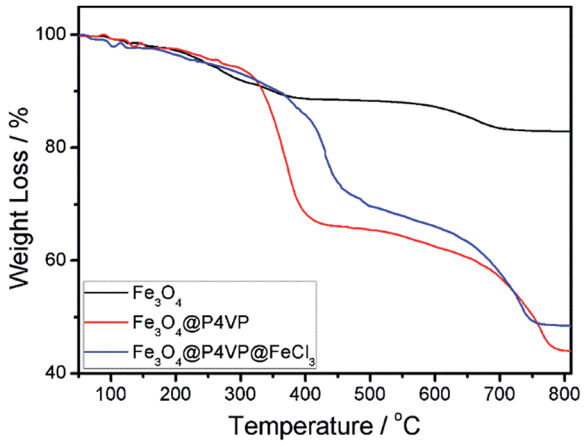

Fig. 6 TGA of (a) Fe_3O_4, (b) Fe_3O_4@P4VP and (c) Fe_3O_4@P4VP@$FeCl_3$.

crystalline nature of the polymeric shell (Fig. 4b). As expected, the introduction of the $FeCl_3$ to the Fe_3O_4@P4VP nanostructure did not affect the crystalline structures of Fe_3O_4@P4VP significantly. The high chemical stability of Fe_3O_4 and P4VP ensures the structure integration in presence of acidic $FeCl_3 \cdot 6H_2O$.

The FTIR spectrum of the product is shown in Fig. 5. The relatively high intensity of the band at 592 cm^{-1} is characteristic of the Fe–O vibrations. The characteristic absorption of the band at 1707 and 1165 cm^{-1} corresponds to the C=O stretching of the carboxylic acid group and in-plane deformation of C–O–H stretching, which proves that –COOH functional groups are located on the surface of Fe_3O_4 nanoparticles (Fig. 5a). In the FTIR spectrum of Fe_3O_4@P4VP microspheres, the characteristic absorptions at 1603, 1562, and 1417 cm^{-1} are attributed to the vibration of the pyridine ring. The band at 1603 cm^{-1} corresponds to the stretching vibration absorption of the C–N bond, and the bands at around 1562 and 1417 cm^{-1} are attributed to the stretching vibration absorption of the C=C bond, which further prove the encapsulation of P4VP on the surface of the Fe_3O_4 particles (Fig. 5b). Furthermore, a new peak was observed at 1627 cm^{-1} after the introduction of the $FeCl_3$ moiety, which shows chemical interaction between the iron and the polymer (Fig. 5c).

The thermal stability of the Fe_3O_4, Fe_3O_4@P4VP and Fe_3O_4@P4VP@$FeCl_3$ nanostructures was also examined by TGA in the temperature range of 50–800 °C (Fig. 6). The mass loss of Fe_3O_4 was due to the decomposition of organic PAA layer on the surface of Fe_3O_4 microspheres (Fig. 6a). Fe_3O_4@P4VP microspheres show two steps of mass loss. The first one, from room temperature to 440 °C, is related to the desorption of adsorbed water and the degradation of secondary nucleation polymer chains on the surface of microsphere. The second loss, from 440 to 800 °C, is instead correlated to the polymer shell and the PAA modification on the Fe_3O_4 (Fig. 6b). For the Fe_3O_4@P4VP@$FeCl_3$ catalyst, the main decomposition stage was similar to Fe_3O_4@P4VP microspheres. The results demonstrated that the

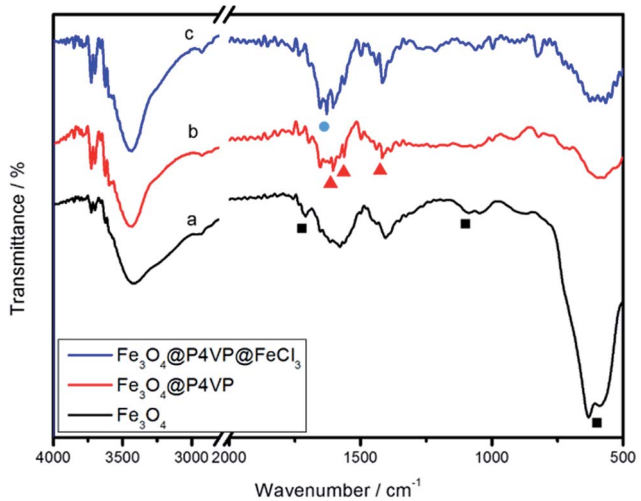

Fig. 5 FTIR spectra of (a) Fe_3O_4, (b) Fe_3O_4@P4VP and (c) Fe_3O_4@P4VP@$FeCl_3$.

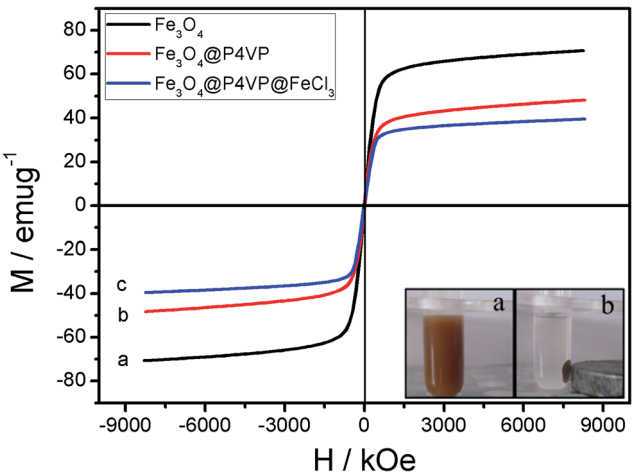

Fig. 7 Room-temperature magnetic hysteresis loops of (a) Fe_3O_4, (b) Fe_3O_4@P4VP and (c) Fe_3O_4@P4VP@$FeCl_3$. Photos of the insets depict magnetic recycling of Fe_3O_4@P4VP@$FeCl_3$ catalyst.

Fe_3O_4@P4VP@$FeCl_3$ catalyst is thermally stable under the conditions of the aerobic oxidation reaction.

The magnetic performance of the Fe_3O_4@P4VP@$FeCl_3$ core–shell nanostructure was investigated by SQUID at room temperature. The magnetization curves of synthesized samples are shown in Fig. 7. The magnetization curves of composite nanospheres exhibit no remanence at room temperature. Again, the results indicate their superparamagnetism, which is crucial for controllable flocculation and dispersion in solution by an external magnetic field. A saturation magnetization value of the Fe_3O_4@P4VP nanospheres of 47.2 emu g^{-1} ensures its rapid recoverability as catalyst support under an external magnetic field. The value is lower than that of Fe_3O_4 nanoparticles (70.8 emu g^{-1}) due to the capsulation of magnetic components into the P4VP. In addition, Fe_3O_4@P4VP@$FeCl_3$ catalyst could be easily recovered by an external magnetic field as shown in Fig. 7; its saturation magnetization value is 39.8 emu g^{-1}.

The high resolution XPS spectra is obtained and the results are shown in Fig. 8, which shows the XPS spectra of the Fe_3O_4@P4VP@$FeCl_3$ core–shell structure. The strong peaks in the Fe_3O_4@P4VP@$FeCl_3$ signal are attributed to the N 1s and C 1s binding energies, respectively. The binding energies at 711 and 55 eV belong to the Fe 3p and Fe $2p_{2/3}$, respectively. The peaks at 268 and 198 eV are due to the existence of Cl 2p and Cl 2s binding, respectively. The results strongly indicate the existence of iron(III) moieties on the surface of the Fe_3O_4@P4VP@$FeCl_3$ catalyst.

The catalytic activity of the synthesized Fe_3O_4@P4VP@$FeCl_3$ toward the aerobic oxidation reaction was evaluated employing alcohol substrates and using TEMPO as the radical initiator. The control experiment showed that no benzaldehyde was detected in absence of catalyst (Table 1, entry 1). Also, the employment of Fe_3O_4 and Fe_3O_4@P4VP as catalysts failed to oxidize any benzyl alcohol to its corresponding aldehyde (Table 1, entries 2 and 3). Homogeneous iron catalysts were evaluated and almost quantitative conversion was observed. However, slightly lowered selectivity was observed due to overoxidation to benzoic acid (Table 1, entries 4–5). The amount of Fe_3O_4@P4VP@$FeCl_3$ added in this reaction was 2 mol%, based on the same iron loading; quantitative yields were achieved using KNO_2 additive (Table 1, entry 6). Several additives were tested under the same reaction conditions and KNO_2 was the most optimal one. Basic inorganic additives were tested and only low to medium yields were achieved (Table 1, entries 7–8). A basic organic additive was evaluated but a poor yield was observed (Table 1, entry 9). Further solvent screening showed that CH_3CN is the most suitable solvent for the aerobic oxidation of benzyl alcohol in the presence of Fe_3O_4@P4VP@$FeCl_3$ (Table 1, entries 6, 10–12). Aromatic solvents such as toluene gave lower yields (Table 1, entry 10). Moreover, oxygen containing solvents, such as THF and ethanol, provided much lower yield, presumably due to their ability to excessively coordinate the metal (Table 1, entries 11 and 12).

Table 1 Reaction condition optimization using benzyl alcohol[a]

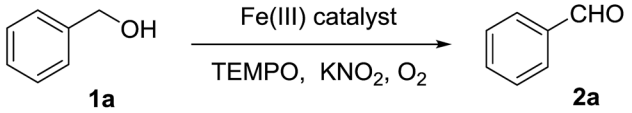

1a 2a

Entry	Catalyst	Solvent	Additive	Selec.[b]	Yield[b]
1	—	CH_3CN	—	—	<5%
2	Fe_3O_4	CH_3CN	KNO_2	—	<5%
3	Fe_3O_4@P4VP	CH_3CN	KNO_2	—	<5%
4	$FeCl_3 \cdot 6H_2O$	CH_3CN	KNO_2	91%	99%
5	$Fe(NO_3)_3$	CH_3CN	KNO_2	78%	99%
6	Fe_3O_4@P4VP@$FeCl_3$	CH_3CN	KNO_2	99%	99%
7	Fe_3O_4@P4VP@$FeCl_3$	CH_3CN	$NaHCO_3$	99%	76%
8	Fe_3O_4@P4VP@$FeCl_3$	CH_3CN	Na_2CO_3	99%	68%
9	Fe_3O_4@P4VP@$FeCl_3$	CH_3CN	Pyridine	99%	43%
10	Fe_3O_4@P4VP@$FeCl_3$	$PhCH_3$	KNO_2	95%	71%
11	Fe_3O_4@P4VP@$FeCl_3$	THF	KNO_2	99%	55%
12	Fe_3O_4@P4VP@$FeCl_3$	EtOH	KNO_2	99%	21%

[a] Reaction conditions: 1.0 mmol of benzyl alcohol, 2 mol% of iron catalyst, 5.0 mL of solvent, 0.2 mmol of TEMPO and 0.2 mmol of additive; 60 °C, 12 h under 1 atm O_2. [b] Selectivities and yields were calculated by GC-MS using nitrobenzene as the internal standard.

With the optimal reaction conditions in hand, a variety of alcohol substrates were tested using Fe_3O_4@P4VP@$FeCl_3$ core–shell catalyst. Benzyl alcohol was transformed to the corresponding benzaldehyde in 99% yield after 12 h (Table 2, entry 1). For the aerobic oxidation of benzyl alcohol in presence of Fe_3O_4@P4VP@$FeCl_3$ as the catalyst, the turnover number (TON) was calculated to be 50. *p*-Methyl benzyl alcohol and *p*-methoxy benzyl alcohol were reactive as electron-rich benzyl alcohols under the optimal reaction conditions, affording 99% and 95% yield, respectively (Table 2, entries 2 and 3). Alcohol substrates bearing electron-withdrawing functional groups, such as *p*-fluorobenzyl alcohol, were also tolerated. A slightly lowered yield was observed due to the reduction in electron efficiency (Table 2, entry 4). The heterocyclic alcohol pyridin-2-ylmethanol was selectively converted to its corresponding aldehyde, in the presence of the Fe derived core–shell catalyst (Table 2, entry 5). Moreover, cinnamaldehyde was obtained in good yield starting from the corresponding allylic alcohol (Table 2, entry 6). The

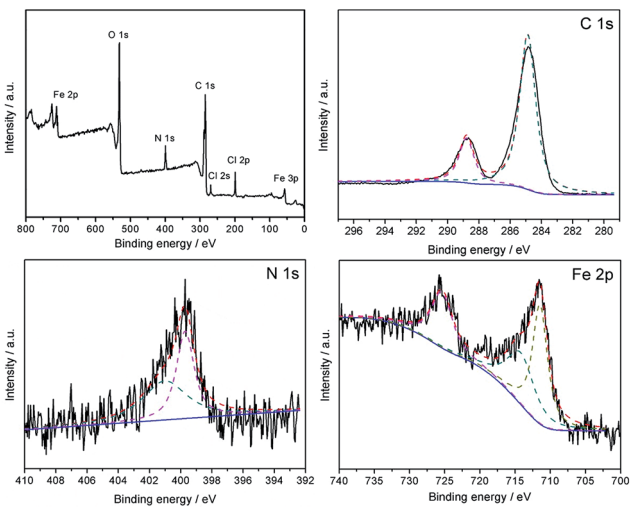

Fig. 8 XPS Spectra of Fe_3O_4@P4VP@$FeCl_3$.

Table 2 Aerobic oxidation of a variety of alcohols[a]

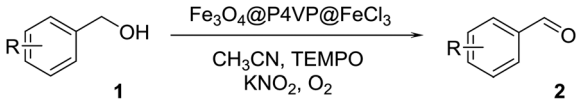

Entry	Alcohol	Product	Sel.	Yield
1	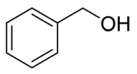	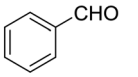	99%	99%
2	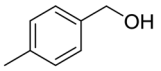	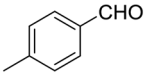	99%	99%
3	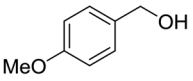	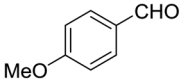	99%	95%
4	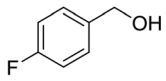	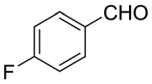	81%	80%
5	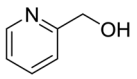	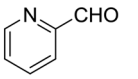	99%	99%
6	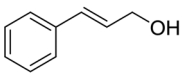	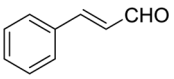	95%	94%
7	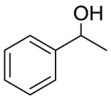	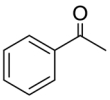	51%	50%
8	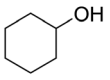		24%	22%

[a] Reaction conditions: 1.0 mmol of benzyl alcohol, 2 mol% of Fe_3O_4@P4VP@$FeCl_3$ catalyst, 5.0 mL of CH_3CN, 0.2 mmol of TEMPO and 0.2 mmol of additive; 60 °C, 12 h under 1 atm O_2.

Table 3 Benzylic oxidation in presence of different additives[a]

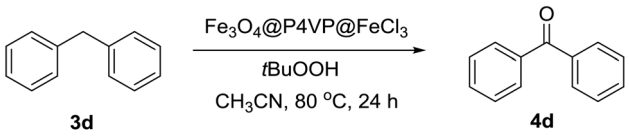

Entry	Catalyst	Additive	Selec.	Yield[b]
1	$FeCl_3 \cdot 6H_2O$	None	—	<5%
2	$FeCl_3 \cdot 6H_2O$	Pyridine	99%	91%
3	$Fe(NO_3)_3 \cdot 9H_2O$	None	—	<5%
4	$Fe(NO_3)_3 \cdot 9H_2O$	Pyridine	99%	75%
5	Fe_3O_4@P4VP@$FeCl_3$	None	99%	84%
6	Fe_3O_4@P4VP@$FeCl_3$	Pyridine	99%	99%
7[c]	Fe_3O_4@P4VP@$FeCl_3$	Pyridine	99%	99%
8	Fe_3O_4@P4VP@$FeCl_3$	Et_3N	99%	85%
9	Fe_3O_4@P4VP@$FeCl_3$	HMTA	99%	87%

[a] Reaction conditions: 1.0 mmol **3d**, 2.0 mol% Fe_3O_4@P4VP@$FeCl_3$ catalyst, 5 mol% additive, 3.0 mmol TBHP, 2.0 mL acetonitrile, 80 °C for 24 h. [b] Isolated yield. [c] 2 mol% pyridine.

transformation of secondary alcohols to ketones is also highly important in synthetic chemistry; 1-phenylethanol and cyclohexanol were both tested as secondary alcohols (Table 2, entries 7 and 8). Unfortunately, only 50% and 22% of acetophenone and cyclohexanone respectively were obtained.

The oxidation of diphenylmethane **3a** for the generation of benzophenone **4a** was carried out in 2.0 mL acetonitrile at 80 °C for 24 h (Table 3). The activation of C–H bond is difficult and *tert*-butyl hydroperoxide (TBHP) was employed as the oxidant under extended reaction time. The catalytic system has been re-optimized to adapt the benzylic oxidation reaction of hydrocarbon derivatives. In the absence of any additive, $FeCl_3 \cdot 6H_2O$ and $Fe(NO_3)_3 \cdot 9H_2O$ failed to promote any conversion (Table 3, entries 1 and 3). The employment of basic pyridine additive strongly increased the yield of the desired benzophenone product (Table 3, entries 2 and 4). Initially, 91% conversion and 99% selectivity were obtained for Fe_3O_4@P4VP@$FeCl_3$ catalyst in the absence of additive (Table 1, entry 5). The high efficiency of Fe_3O_4@P4VP@$FeCl_3$ catalyst was due to the pyridine sites on the surface of the heterogeneous iron catalyst. The addition of a small amount of homogeneous pyridine can further boost the conversion to over 99% (Table 1, entry 6). Furthermore, the amount of pyridine can be reduced to 2 mol% without affecting the yield and selectivity of the diphenylmethane oxidation (Table 1, entry 7). In addition, other basic additives were examined. However, almost no improvement was observed when triethylamine (Et_3N) was employed (Table 3, entry 8). Hexamethylenetetramine (HMTA) failed to increase the yield as well (Table 3, entry 9). These results indicate that pyridine was the best base additive among the organic bases screened. Our Fe_3O_4@P4VP@$FeCl_3$ catalyst was designed so that the heterogeneous P4VP layer would provide large amounts of pyridine sites. These heterogeneous pyridine sites were highly helpful for the oxidation reaction process, while homogeneous $FeCl_3$ failed to convert diphenylmethane to the desired product. Several organic solvents were screened and acetonitrile demonstrated good compatibility in the catalytic system, which resulted in 99% isolated yield (Table 3, entry 2). Other solvents showed a trend similar to the results in Table 1. Therefore the optimal catalytic system was set to be 2.0 mol% Fe_3O_4@P4VP@$FeCl_3$ catalyst, 0.02 equivalent of pyridine additive and 3.0 equivalents of TBHP in acetonitrile solvent.

The optimized reaction conditions were utilized for the oxidation of other substrates in the presence of *t*BuOOH (Table 4). C–H activation/oxidation was further extended to other hydrocarbon compounds. Ethylbenzene **3a** was oxidized to 1-phenylethanone **4a** in 91% conversion and 97% selectivity (Table 4, compound **4a**). Ethylthiophene **3b** containing a heterocyclic moiety was also employed as the substrate and over 96% yield and up to 99% selectivity were achieved (Table 3,

Table 4 Benzylic oxidation of hydrocarbon derivatives

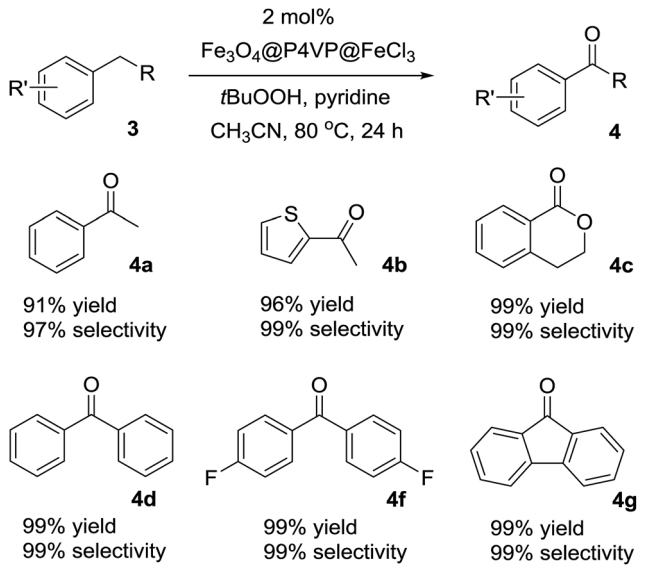

compound **4b**). Isochromane **3c** underwent oxidation to give 4-isochromanone **4c** in high yield (Table 4, compound **4c**). The oxidation of diphenylmethane **3d** and bis(4-fluorophenyl) methanone **3f** for the generation of corresponding ketones **4d** and **4f** were smooth (Table 4, compounds **4d** and **4f**). Moreover, by oxidation of 9*H*-fluorene **3g**, the reaction proceeded smoothly to form the corresponding ketones in high yield and selectivity (Table 4, compound **4g**). In summary, the Fe_3O_4@P4VP@$FeCl_3$ was a versatile catalyst for benzylic methylene compounds (Table 4).

The recyclability of the catalyst was studied under the optimized conditions and utilizing 2 mol% and 0.5 mol% of Fe_3O_4@P4VP@$FeCl_3$ catalyst in acetonitrile (Fig. 9). The same batch of the Fe_3O_4@P4VP@$FeCl_3$ catalyst was reused for five catalytic cycles. Conversion and selectivity were retained at 99% and the yield of benzaldehyde was compromised only slightly

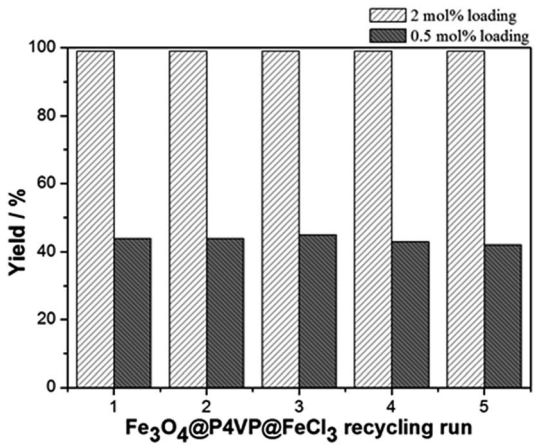

Fig. 9 Core-shell iron catalyst recyclability test at 2 mol% and 0.5 mol% catalyst loading for aerobic oxidation of benzyl alcohol.

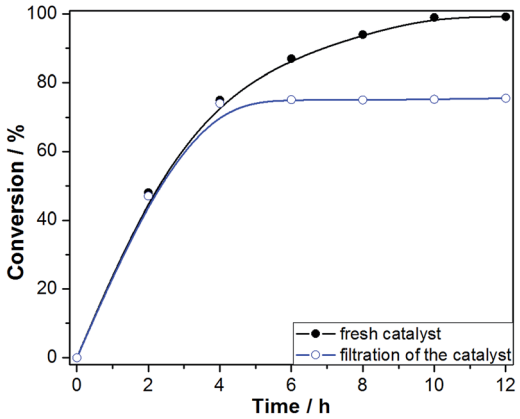

Fig. 10 Hot filtration test of Fe_3O_4@P4VP@$FeCl_3$ in aerobic oxidation of benzyl alcohol.

after five cycles (Fig. 9). At a lower catalyst loading of 0.5 mol%, 44% yield was achieved in the initial cycle. Only slight yield decrease (98%) was observed after 5 cycles of reaction (Fig. 9). The ability to retain conversion rates and selectivities after five cycles indicates that the core–shell heterogeneous catalyst is highly stable. TEM and p-XRD spectra showed no significant difference between fresh Fe_3O_4@P4VP@$FeCl_3$ and five-time reused samples (Fig. S1 and S2†).

The hot filtration test was conducted to confirm the heterogeneous nature of the catalytic aerobic oxidation and low reaction leaching (Fig. 10). The Fe_3O_4@P4VP@$FeCl_3$ catalyst was isolated using an external magnet after 4 hours of reaction and the mixture was stirred for another 8 h. Conversion of benzyl alcohol stopped after the catalyst was removed at 4 h reaction time. This result indicates that the multi-dentate Fe⋯N bonds ensure the stability of the Fe_3O_4@P4VP@$FeCl_3$ catalyst during the liquid oxidation process. Furthermore, the reaction solution after solid catalyst removal was tested by ICP-AES, which suggested 2.3 ppm of iron content. These results demonstrated the high stability of Fe_3O_4@P4VP@$FeCl_3$ core–shell catalyst during the oxidation reaction condition.

Several control experiments were designed and conducted in order to reveal the reaction mechanism. First of all, the oxidation reaction was carried out without TEMPO (Scheme 1, reaction 1). In the absence of radical initiator, reaction was not able to proceed. This observation suggested radical reaction

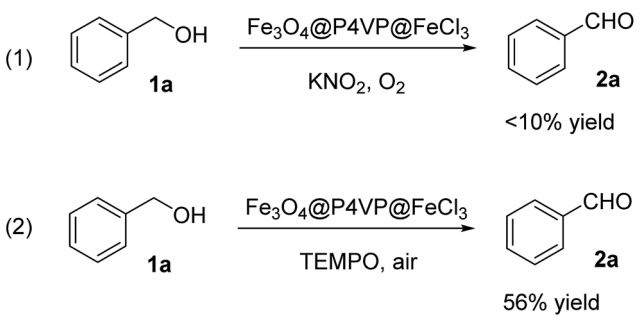

Scheme 1 Controlled experimental reaction.

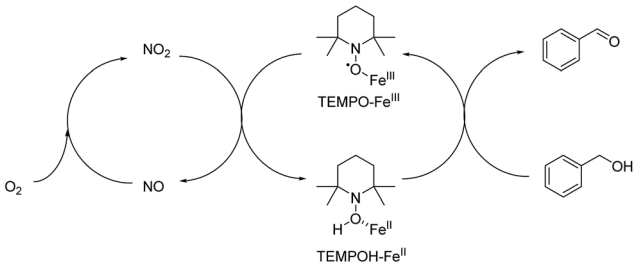

Fig. 11 Reaction mechanism of Fe(III) promoted oxidation.

pathway. Furthermore, reaction was performed under open air condition, decent yield of the desired aldehyde product was obtained (Scheme 1, reaction 2). Oxygen was crucial in the oxidation process and the certain density of oxygen ensures the high conversion of the alcohol product.

A overall mechanism of Fe(III) promoted catalytic oxidation can be described as a redox reaction involving two separated cycles in Fig. 11. KNO_2 was acting as a source of NO_2. Therefore, TEMPO is envisioned to carry out the main oxidation reaction of alcohols with the help of Fe(III) that initiates a series of electron and proton transfer steps in the right cycle where TEMPO-Fe(III) is reduced to generate TEMPOH-Fe(II). The overall oxidation process involves the oxidation of Fe(II) to Fe(III) by NO_2 and the oxidation of TEMPOH to TEMPO by Fe(III). The conversion of NO to NO_2 was performed in the presence of molecular oxygen.

4. Conclusions

In summary, a novel magnetic core–shell Fe_3O_4@P4VP@$FeCl_3$ structure was designed, prepared and fully characterized. The iron(III) immobilized core–shell microspheres were composed by a magnetic Fe_3O_4 core and a P4VP middle layer. Taking advantage of active iron(III) catalytic site, the magnetic composite microspheres were utilized as an efficient catalyst for the selective aerobic oxidation of alcohols. A variety of alcohol substrates were tolerated under our optimized conditions at only 2 mol% catalyst loading. In addition, benzylic oxidation of hydrocarbon compounds was also carried out using the Fe_3O_4@P4VP@$FeCl_3$ catalyst and *t*BuOOH oxidant. The initial catalytic activity of the Fe_3O_4@P4VP@$FeCl_3$ catalyst was retained after at least five consecutive reaction cycles. A hot filtration test suggested low leaching of iron into the solution. Further applications of the various heterogeneous core–shell catalysts are currently under investigation.

Conflicts of interest

There are no conflicts to declare.

Acknowledgements

This work is supported by Beijing Natural Science Foundation (2172037) and National Natural Science Foundation of China (No. 51503016). P. Y. thanks the State Key Laboratory of Chemical Resource Engineering and Y. L. thanks the Fundamental Research Funds for the Central Universities (Grant No. FRF-TP-16-004A3) for funding support.

Notes and references

1 Q. Cao, L. M. Dornan, L. Rogan, N. L. Hughes and M. J. Muldoon, *Chem. Commun.*, 2014, **50**, 4524–4543.
2 (*a*) R. A. Sheldon, *Catal. Today*, 2015, **247**, 4; (*b*) C. Parmeggiani and F. Cardona, *Green Chem.*, 2012, **14**, 547; (*c*) Z. Shi, C. Zhang, C. Tang and N. Jiao, *Chem. Soc. Rev.*, 2012, **41**, 3381; (*d*) Q. Cao, L. M. Dornan, L. Rogan, N. L. Hughes and M. J. Muldoon, *Chem. Commun.*, 2014, **50**, 4524; (*e*) M. J. Schultz and M. S. Sigman, *Tetrahedron*, 2006, **62**, 8227.
3 (*a*) Z. Guo, B. Liu, Q. Zhang, W. Deng, Y. Wang and Y. Yang, *Chem. Soc. Rev.*, 2014, **43**, 3480; (*b*) S. E. Devis, M. S. Lde and R. J. Davis, *Green Chem.*, 2013, **15**, 17.
4 Z. Guo, B. Liu, Q. Zhang, W. Deng, Y. Wang and Y. Yang, *Chem. Soc. Rev.*, 2014, **43**, 3480–3524.
5 M. Hajimohammadi, N. Safari, H. Mofakham and F. Deyhimi, *Green Chem.*, 2011, **13**, 991.
6 B. Chen, L. Wang and S. Gao, *ACS Catal.*, 2015, **5**, 5851–5876.
7 (*a*) P. Miedziak, M. Sankar, N. Dimitratos, J. A. Lopez-Sanchez, A. F. Carley, D. W. Knight, S. H. Taylor, C. J. Kiely and G. J. Hutchings, *Catal. Today*, 2011, **164**, 315; (*b*) Y. Li, Y. Gao and C. Yang, *Chem. Commun.*, 2015, **51**, 7721; (*c*) X. Yu, Y. Huo, J. Yang, S. Chang, Y. Ma and W. Huang, *Appl. Surf. Sci.*, 2013, **280**, 450; (*d*) R. H. Adnan, G. G. Andersson, M. I. J. Polson, G. F. Metha and V. B. Golovko, *Catal. Sci. Technol.*, 2015, **5**, 1323; (*e*) T. Wang, X. Yuan, S. Li, L. Zeng and J. Gong, *Nanoscale*, 2015, **7**, 7593; (*f*) C. D. Pina, E. Falletta, L. Prati and M. Rossi, *Chem. Soc. Rev.*, 2008, **37**, 2077.
8 (*a*) K. M. Gligorich and M. S. Sigman, *Chem. Commun.*, 2009, 3854; (*b*) Y. Ye, M. D. Johnson, T. Diao, M. H. Yates and S. S. Stahl, *Green Chem.*, 2010, **12**, 1180; (*c*) B. Karimi, S. Abedi, J. H. Clark and V. Budarin, *Angew. Chem., Int. Ed.*, 2006, **45**, 4776; (*d*) B. Karimi, A. Zamani, S. Abedi and J. H. Clark, *Green Chem.*, 2009, **11**, 109; (*e*) D. Sahu, C. Sarmah and P. Das, *Tetrahedron Lett.*, 2014, **55**, 3422; (*f*) S. F. J. Hackett, R. M. Brydson, M. H. Gass, I. Harvey, A. D. Newman, K. Wilson and A. F. Lee, *Angew. Chem., Int. Ed.*, 2007, **46**, 8593; (*g*) H. Wu, Q. Zhang and Y. Wang, *Adv. Synth. Catal.*, 2005, **347**, 1536; (*h*) X. Ye, M. D. Johnson, T. Diao, M. H. Yates and S. S. Stahl, *Green Chem.*, 2010, **12**, 1180; (*i*) B. Karimi, D. Elhamifar, J. H. Clark and A. J. Hunt, *Org. Biomol. Chem.*, 2011, **9**, 7420; (*j*) H. Yang, X. Han, Z. Ma, R. Wang, J. Liu and X. Ji, *Green Chem.*, 2010, **12**, 441; (*k*) C. M. A. Parlett, D. W. Bruce, N. S. Hondow, A. F. Lee and K. Wilson, *ACS Catal.*, 2011, **1**, 636; (*l*) J. Chen, Q. Zhang, Y. Wang and H. Wan, *Adv. Synth. Catal.*, 2008, **350**, 453; (*m*) B. Karimi, A. Zamani and J. H. Clark, *Organometallics*, 2005, **24**, 4695; (*n*) M. J. Schultz, C. C. Park and M. S. Sigman, *Chem. Commun.*, 2002, 3034.
9 (*a*) Y. Hong, X. Yan, X. Liao, R. Li, X. Xu, L. Xiao and J. Fan, *Chem. Commun.*, 2014, **50**, 9679; (*b*) T. Lu, Z. Du, J. Liu, H. Ma

and J. Xu, *Green Chem.*, 2013, **15**, 2215; (*c*) T. Wang, H. Shou, Y. Kou and H. Liu, *Green Chem.*, 2009, **11**, 562; (*d*) K. Kon, S. M. A. H. Siddiki and K.-i. Shimizu, *J. Catal.*, 2013, **304**, 63; (*e*) T. Wang, C.-X. Xiao, L. Yan, L. Xu, J. Luo, H. Shou, Y. Kou and H. Liu, *Chem. Commun.*, 2007, 4375.

10 (*a*) A. Wusiman and C.-D. Lu, *Appl. Organomet. Chem.*, 2015, **29**, 254; (*b*) J. Olguin, H. Muller-Bunz and M. Albrecht, *Chem. Commun.*, 2014, **50**, 3488; (*c*) L. Liu, M. Yu, B. B. Wayland and X. Fu, *Chem. Commun.*, 2010, **46**, 6353.

11 (*a*) K. Yamaguchi and N. Mizuno, *Angew. Chem., Int. Ed.*, 2002, **41**, 4538; (*b*) Z. W. Yang, X. Zhao, T. J. Li, W. L. Chen, Q. X. Kang, X. Q. Xu, X. X. Liang, Y. Feng, H. H. Duan and Z. Q. Li, *Catal. Commun.*, 2015, **65**, 34; (*c*) D. Canseco-Gonzalez and M. Albrecht, *Dalton Trans.*, 2013, **42**, 7424.

12 (*a*) B. Xu, J. P. Lumb and B. A. Arndtsen, *Angew. Chem., Int. Ed.*, 2015, **54**, 4208; (*b*) L. Vanoye, M. Pablos, C. D. Bellefon and A. Favre-Reguillon, *Adv. Synth. Catal.*, 2015, **357**, 739; (*c*) B.-T. Chen, K. V. Bukhryakov, R. Sougrat and V. O. Rodionov, *ACS Catal.*, 2015, **5**, 1313; (*d*) G. Zhang, C. Yang, E. Liu, L. Li, J. A. Golen and A. L. Rheingold, *RSC Adv.*, 2014, **4**, 61907; (*e*) P. Gamez, I. W. C. E. Arends, J. Reedijk and R. A. Sheldon, *Chem. Commun.*, 2003, 2414–2415; (*f*) G. Zhang, X. Han, Y. Luan, Y. Wang, X. Wen, L. Xu, C. Ding and J. Gao, *RSC Adv.*, 2013, **3**, 9255; (*g*) S. Samanta, S. Das, P. K. Samanta, S. Dutta and P. Biswas, *RSC Adv.*, 2013, **3**, 19455.

13 S. E. Martin and D. F. Suarez, *Tetrahedron Lett.*, 2002, **43**, 4475.

14 N. Wang, R. Liu, J. Chen and X. Liang, *Chem. Commun.*, 2005, 5322.

15 J. Liu and S. Ma, *Org. Lett.*, 2013, **15**, 5150.

16 (*a*) M. A. Chari and K. Syamasundar, *Synthesis*, 2005, **5**, 0708–0710; (*b*) M. R. Farsani and B. Yadollahi, *J. Mol. Catal. A: Chem.*, 2014, **392**, 8–15; (*c*) Y. Kuang, Y. Nabae, T. Hayakawa and M. Kakimoto, *Appl. Catal., A*, 2012, **423–424**, 52–58; (*d*) P. Das, N. Aggarwal and N. R. Guha, *Tetrahedron Lett.*, 2013, **54**, 2924–2928.

17 F. Rajabi, A. Pineda, S. Naserian, A. M. Balu, R. Luque and A. A. Romero, *Green Chem.*, 2013, **15**, 1232.

18 M. Mahyari and A. Shaabani, *Appl. Catal., A*, 2014, **469**, 524.

19 P. R. Likhar, R. Arundhathi, S. Ghosh and M. L. Kantam, *J. Mol. Catal. A: Chem.*, 2009, **302**, 142–149.

20 J. Mao, X. Hu, H. Li, Y. Sun, C. Wang and Z. Chen, *Green Chem.*, 2008, **10**, 827–831.

21 R. G. Chaudhuri and S. Paria, *Chem. Rev.*, 2012, **112**, 2373–2433.

22 M. B. Gawande, A. Goswami, T. Asefa, H. Guo, A. V. Biradar, D. L. Peng, R. Zboril and R. S. Varma, *Chem. Soc. Rev.*, 2015, **44**, 7540–7590.

23 (*a*) C. Hui, C. Shen, J. Tian, L. Bao, H. Ding, C. Li, Y. Tian, X. Shi and H. J. Gao, *Nanoscale*, 2011, **3**, 701–705; (*b*) Y. D. Chiang, S. Dutta, C. T. Chen, Y. T. Huang, K. S. Lin, J. C. S. Wu, N. Suzuki, Y. Yamauchi and K. C. W. Wu, *ChemSusChem*, 2015, **8**, 789–794.

24 (*a*) Q. Zhang, I. Lee, J. B. Joo, F. Zaera and Y. Yin, *Acc. Chem. Res.*, **46**, 1816–1824; (*b*) P. Hu, J. V. Morabito and C. K. Tsung, *ACS Catal.*, 2014, **4**, 4409–4419; (*c*) Y. Long, M. Xie, J. Niu, P. Wang and J. Ma, *Appl. Surf. Sci.*, 2013, **277**, 288–292; (*d*) X. Zhang, J. Wu, G. Meng, X. Guo, C. Liu and Z. Liu, *Appl. Surf. Sci.*, 2016, **366**, 486–493; (*e*) Z. Sun, H. Li, G. Cui, Y. Tian and S. Yan, *Appl. Surf. Sci.*, 2016, **360**, 252–262.

25 H. Deng, X. Li, Q. Peng, X. Wang, J. Chen and Y. Li, *Angew. Chem., Int. Ed.*, 2005, **44**, 2782–2785.

